

AJK2015- 06342

CFD VALIDATION EXPERIMENT OF A MACH 2.5 AXISYMMETRIC SHOCK-WAVE/BOUNDARY-LAYER INTERACTION

David O. Davis
NASA Glenn Research Center
Cleveland, OH, USA

ABSTRACT

Preliminary results of an experimental investigation of a Mach 2.5 two-dimensional axisymmetric shock-wave/boundary-layer interaction (SWBLI) are presented. The purpose of the investigation is to create a SWBLI dataset specifically for CFD validation purposes. Presented herein are the details of the facility and preliminary measurements characterizing the facility and interaction region. These results will serve to define the region of interest where more detailed mean and turbulence measurements will be made.

INTRODUCTION

Experimental investigations of specific flow phenomena can provide great insight into the flow behavior but often lack the necessary detail and documentation to be useful as CFD validation experiments. Reasons for this include, but are not limited to:

- Undefined boundary conditions
- Inconsistent results
- Undocumented 3D effects (centerline only measurements)
- Lack of uncertainty analysis

In 1994, Settles and Dodson [1], [2] reviewed a large number of supersonic and hypersonic experiments and evaluated them for suitability to be used as CFD validation experiments. Of the hundreds of experiments reported in the open literature, over one hundred were subjected to rigorous acceptance criteria. Of these, only nineteen (12 supersonic, 7 hypersonic) were deemed to be acceptable for CFD validation. Aeschliman and Oberkampf [3] recognized the need to develop a specific methodology for experimental studies intended specifically for validation purposes.

SWBLI CFD validation experiments performed in non-circular wind tunnels pose a particularly challenging problem, as streamwise and transverse pressure gradients induced by the SWBLI turn a nominally two-dimensional flow-field into a three-dimensional flow-field [4], [5]. This is illustrated in Figure 1 by oil flow visualization obtained in NASA Glenn Research Center's (GRC) 15x15cm Supersonic Wind Tunnel (SWT) with an M=2.0 oblique SWBLI. The view is of the floor of the tunnel where an impinging/reflected oblique shock wave interacts with the boundary layers on the floor and sidewalls and α is the angle of the shock generator plate. For a weak, unseparated interaction (Figure 1a), the flow remains mostly two-dimensional with a slight bottlenecking of

the limiting wall streamlines in the vicinity of the impingement location. For a stronger, separated interaction, (Figure 1b), centerline

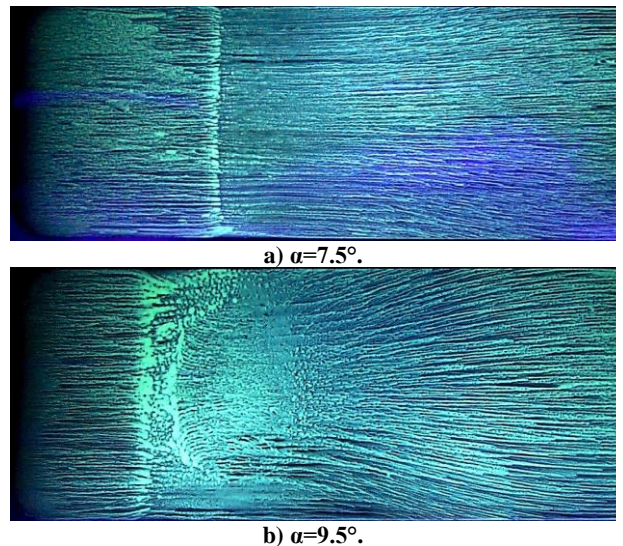


Figure 1. M=2.0 oblique SWBLI oil flow.

measurements alone would not be representative of a two-dimensional interaction and the entire flow-field would need to be surveyed for this case to be useful as a CFD validation case.

The Transformational Tools & Technologies (TTT) Project under NASA's Transformative Aeronautics Concept Program is tasked, in part, with providing quality experiments for the purpose of validating CFD codes and turbulence models. A Mach 2.5 SWBLI has been identified as one of the test cases desired. The primary objective of the current study is to provide a comprehensive dataset for a Mach 2.5 SWBLI that is of sufficient quality to be used as a validation test case.

In order to avoid the pitfalls of a rectangular configuration, an axisymmetric configuration is proposed that is two-dimensional in the mean. The selected interaction is illustrated in Figure 2. A Mach 2.5 core flow approaches a cone-cylinder centerbody that generates a conical shock that impinges and reflects off the cylindrical test section wall, interacting with the naturally occurring test section boundary layer. The

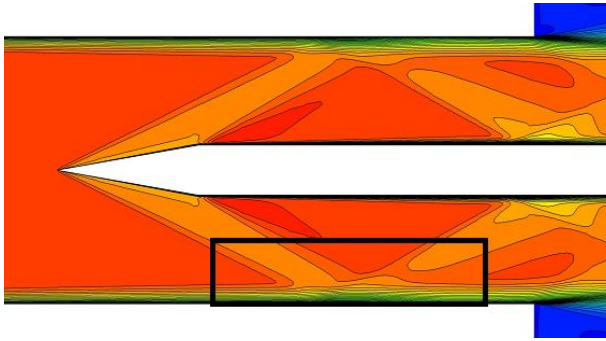


Figure 2. M=2.5 Axisymmetric SWBLI (box indicates region of interest).

approximate measurement area of interest is indicated by the rectangular box shown in the figure. NASA GRC's supersonic facilities, however, all have square or rectangular test sections so a new facility has been designed specifically for this study. This configuration is similar to a study performed by Rose [6], which was considered for Settles and Dodson's validation database, but was rejected due to questions about the accuracy of the hot-wire measurements. A new 17 cm diameter axisymmetric supersonic wind tunnel (Axi-SWT) has been installed in Test Cell W6B and replaces the existing 15x15 cm configuration. The facility design allows for relatively easy changes between the square and circular configurations.

The goal of the initial characterization is to define the interaction region of interest where more refined and redundant measurements will be taken. These measurements will include hot-wire data to quantify the turbulence structure through the interaction region.

NOMENCLATURE

A	= Area
C_D	= Discharge coefficient
C_f	= Skin friction coefficient
CL	= Centerline
D	= Diameter
g_c	= Proportionality constant
H_i	= Incompressible boundary-layer shape factor
L_t	= ASME bellmouth throat length (Figure 5)
M	= Mach number
N	= Number of redundant measurements (Table 1)
p	= Pressure
R	= Radius
R_1	= ASME nozzle ellipse major radius (Figure 5)
R_2	= ASME nozzle ellipse minor radius (Figure 5)
R_c	= Radius of curvature
R_{air}	= Gas constant for air
Re_D	= Reynolds number based on diameter
Re_{D_s}	= Scaled Reynolds number ($Re_{D_s} = Re_D \times 10E-06$)
T	= Temperature or throat tap location (cm, Figure 5)
U	= Velocity
w	= Mass flow rate
x_{sup}	= Axial coordinate relative to C-D nozzle throat (Figure 6)
x, y, z	= Cartesian coordinates
x, r, θ	= Cylindrical coordinates

Greek Symbols

α	= Shock generator cone half-angle (deg)
β	= Ratio of ASME nozzle-to-approach pipe diameter
γ	= Ratio of specific heats for air (1.4)

δ	= Boundary-layer thickness
δ^*	= Boundary-layer displacement thickness
δX_i	= Uncertainty of measurand X_i
θ	= Boundary-layer momentum thickness
μ	= Molecular viscosity
ρ	= Density

Subscripts

0	= Pertaining to plenum conditions
bm	= Pertaining to the ASME bellmouth
e	= Pertaining to boundary-layer edge condition
i	= Pertaining to ideal conditions
noz	= Pertaining to the C-D nozzle
t	= Pertaining to total conditions
th	= Pertaining to throat conditions
ts	= Pertaining to the test section
w	= Pertaining to wall conditions

AXISYMMETRIC SWBLI

As previously mentioned, an axially symmetric SWBLI is the only practical way to ensure a two-dimensional flow in the mean. A number of axisymmetric SWBLIs have been investigated over the years. These include supersonic flow over a double-cone, over a cylinder-flare, an impinging-centerbody SWBLI, and the present configuration of an impinging-duct SWBLI as shown in Figure 3.

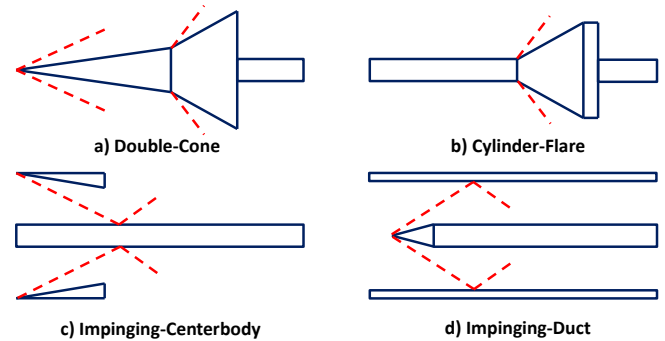


Figure 3. Axisymmetric SWBLI configurations.

The impinging duct configuration was chosen for two reasons. First, inasmuch as the intent of the investigation is to provide CFD validation data, this configuration allows for a relatively thick incoming boundary layer so highly resolved measurements are possible. And second, although not intended to mimic any particular application, it is of the same general configuration as a SWBLI occurring on the cowl surface of axisymmetric inlets with supersonic internal compression. Previous investigations of this flow configuration include the development of integral flow models for solid and porous walls by Seebaugh et al. [7]. An experimental investigation by Seebaugh and Childs [8] presented surface static and flowfield Pitot pressure measurements under Mach 2.82 and 3.78 flow conditions with cone angles of 10, 13 and 15°. Rose [6] acquired detailed turbulence measurements using hot-wire anemometry under Mach 3.88 flow conditions with a 9° cone angle. Neither of the latter two studies, however, were considered to meet the criteria for CFD validation purposes as proposed by Ref. [1].

FACILITY DESCRIPTION

The new 17 cm axisymmetric facility is located in Test Cell W6B at NASA GRC. W6B is a continuous flow supersonic facility with Mach

number variation achieved by interchangeable fixed-geometry nozzle blocks. The plenum chamber is supplied with dry ambient temperature compressed air up to 377 kPa. The exhaust side of the tunnel is connected to lab-wide altitude exhaust which is maintained at less than 13.8 kPa. The 17 cm Axi-SWT utilizes the same plenum chamber and exhaust as NASA GRC's 15x15 cm SWT. A test section diameter of 17 cm was selected so as to maintain similar flow area as the 15x15 cm SWT. Figure 4 shows a section view of both facilities.

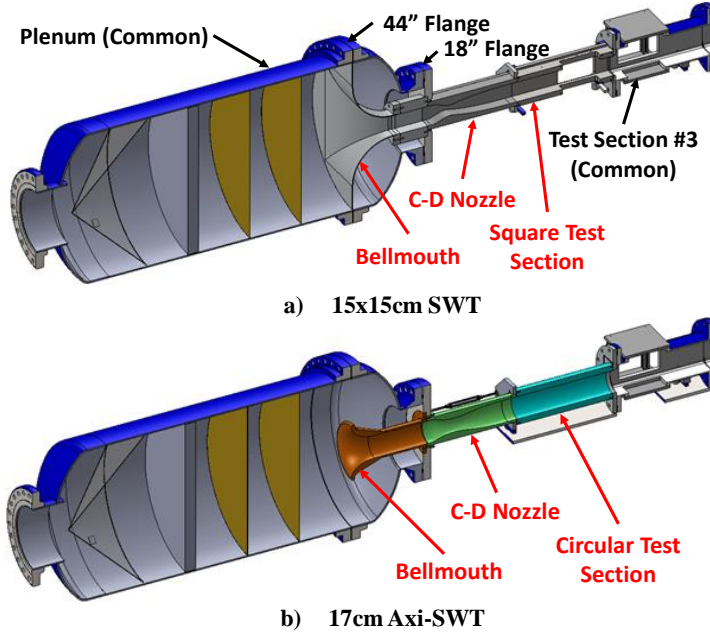


Figure 4. Section view of W6B test facility.

With reference to Figure 4a, installation of the 15x15cm SWT bellmouth requires removal of the 44" flanged bulkhead on the plenum chamber. To allow the facility to be reconfigured between the two configurations with a minimum of effort, the bellmouth for the 17cm Axi-SWT was designed so as to only require removal of the 18" interface flange. A new bellmouth for the 15x15cm SWT is currently in the design cycle to allow similar installation.

As illustrated in Figure 4b, the 17cm Axi-SWT required design and fabrication of three major components: the bellmouth, the convergent-divergent (C-D) supersonic nozzle, and the test section. Beyond these basic components for the facility, the Shock Generator (SG) hardware is also required. A brief description of each component follows.

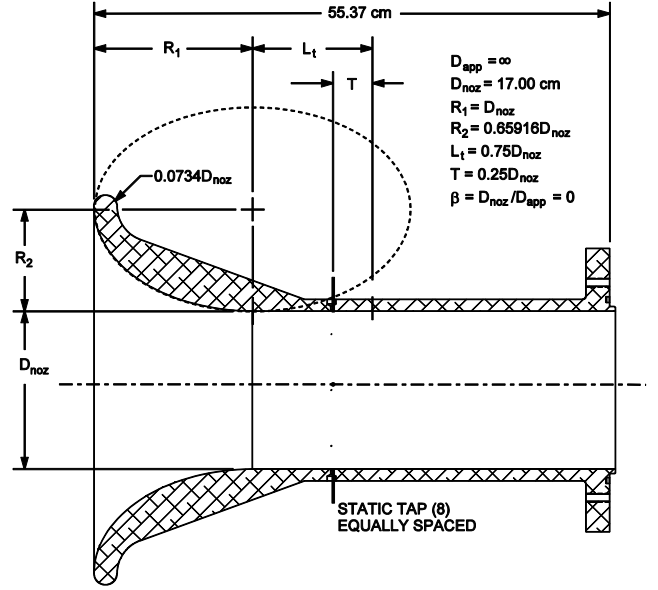
ASME Bellmouth

The bellmouth for the axisymmetric facility serves two purposes. First, it is used to provide a uniform, low Mach number flow to the C-D nozzle, and second, it is used to measure the total mass-flow through the facility:

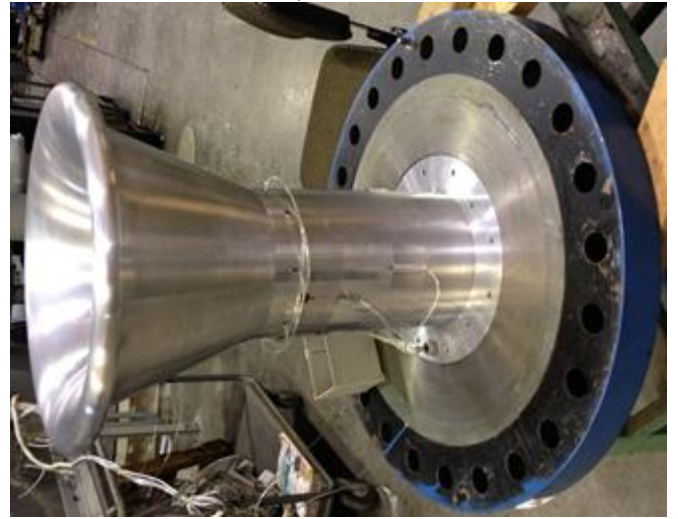
$$\text{Eq. 1} \quad w_{noz} = C_{D,bm} \cdot w_{noz,i}$$

where $w_{noz,i}$ is the ideal mass-flow given by:

$$\text{Eq. 2} \quad w_{noz,i} = \sqrt{\frac{\gamma \cdot g_c}{R_{air}}} \cdot \frac{p_{t,0} \cdot M_{noz} \cdot A_{noz}}{\sqrt{T_{t,0}}} \cdot \left(1 + \frac{\gamma-1}{2} \cdot M_{noz}^2\right)^{\frac{-(\gamma+1)}{2(\gamma-1)}}$$



a) Schematic



b) Hardware

Figure 5. ASME bellmouth.

Geometry: The elliptical bellmouth geometry is based on an ASME Long-Radius Flow Nozzle with throat taps and is a scaled version of similar bellmouths used at NASA GRC. A schematic of the bellmouth and a photo of the actual hardware are shown in Figure 5a and Figure 5b, respectively. This design conforms to the Low- β Nozzle with Throat Taps illustrated in Fig. II-III-14 of Ref. [9] with the following two exceptions. First, no approach pipe exists before the nozzle ($D_{app}=\infty$), hence $\beta=D_{noz}/D_{app}=0$. And second, the nozzle exit flow does not exhaust into a sudden expansion but rather a constant area diffuser.

ASME Nozzle Discharge Coefficient: The discharge coefficient for the bellmouth was determined from a computational calibration performed on a geometrically similar nozzle. The details of the calibration are given in Ref. [10].

$$\text{Eq. 3} \quad C_{D,bm} = C_{D,M=0.5} \cdot f(M)$$

where

$$\text{Eq. 4} \quad C_{D,M=0.5} = 0.993003 - \frac{6.73896}{\sqrt{\text{Re}_{D,bm}}}$$

and

$$\text{Eq. 5} \quad f(M) = 0.999514 \cdot (1 - 0.2M_{bm}^2)^{-0.0086341}$$

and

$$\text{Eq. 6} \quad \text{Re}_{D,bm} = \frac{\rho_{bm} \cdot U_{bm} \cdot D_{bm}}{\mu_{bm}}$$

For the current $M=2.5$ C-D nozzle, the ratio of bellmouth throat area to nozzle throat area ($A_{bm,th}/A_{noz,th}$) is 2.636, so the Mach number in the ASME bellmouth will be approximately $M_{bm,th} = 0.21$.

C-D Nozzle

A schematic of the C-D nozzle is shown in Figure 6. The requirements for the C-D nozzle design include:

- 1) Exit Mach number of 2.5
- 2) Inlet and exit diameter equal (17cm)
- 3) Length approximately the same as 15x15cm nozzles (~66 cm)

The second requirement allows for the C-D nozzle to be replaced with a constant area duct so that the facility can also be run subsonically.

The steps for designing the nozzle include:

- 1) Definition of the inviscid, shock-free supersonic contour.
- 2) Definition of the subsonic contour (contraction).
- 3) Correction of the supersonic contour for B.L. growth.
- 4) Adjustment of the subsonic contour.

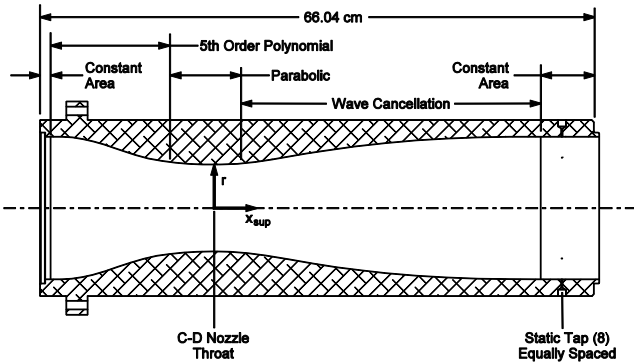


Figure 6. C-D nozzle schematic.

For the first step a Method of Characteristics (MOC) approach was used. To define the inviscid supersonic contour, the exit Mach number, the radius of curvature at the throat ($R_{c,th}$), and a function for the initial expansion are required. To minimize distortion of the sonic line at the throat, $R_{c,th}$ should be large. But as $R_{c,th}$ is increased, the correction for boundary-layer growth becomes more significant and the nozzle length is increased, thus a balance must be achieved. For the current nozzle, given the length constraints, $R_{c,th}$ was selected as:

$$\text{Eq. 7} \quad R_{c,th} = 8.0 \cdot R_{th}$$

where R_{th} is the nozzle radius at the throat. For the initial expansion, a parabolic function was chosen:

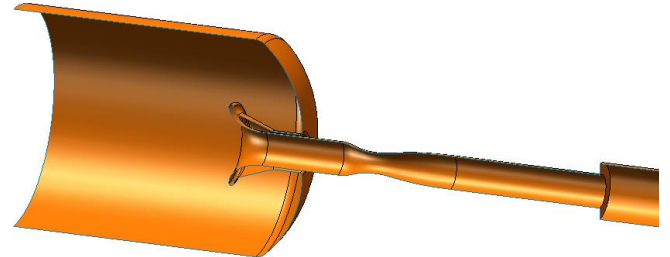
¹ The waves in the boundary-layer thickness (δ) are an artifact of the algorithm used to locate the boundary-layer edge.

$$\text{Eq. 8} \quad \frac{r}{R_{th}} = 1.0 + \left(\frac{R_{th}}{2 \cdot R_{c,th}} \right) \cdot \left(\frac{x_{sup}}{R_{th}} \right)^2$$

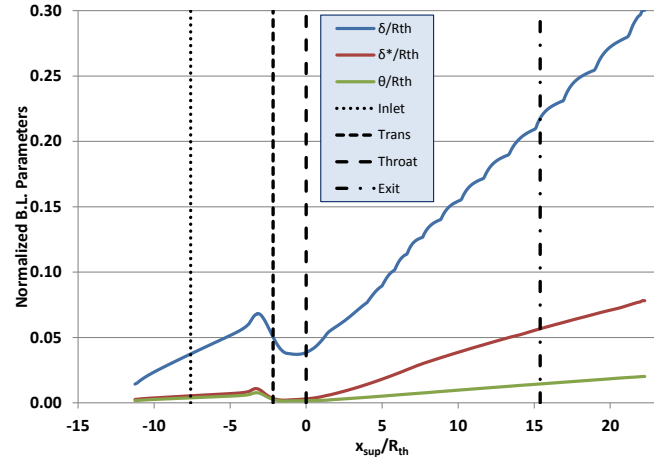
where x_{sup} is the axial coordinate with origin at the inviscid nozzle throat.

For the subsonic contour, the parabolic function for the initial supersonic contour was extended upstream to an arbitrary point. Then a 5th order polynomial function was specified to transition from the upstream constant area section to the parabolic section. A 5th order polynomial allows for continuous second derivatives of the contour.

There are a number of methods available to correct for the boundary-layer growth in a nozzle. The most common is to correct the contour by an estimate of the displacement thickness growth through the nozzle. For this nozzle, we chose to estimate the displacement thickness growth by performing a numerical simulation using the WIND-US flow solver [11] in conjunction with the Menter Shear Stress Transport (SST) turbulence model [12]. With reference to Figure 7a, the computational domain included the plenum tank, ASME bellmouth, C-D nozzle, test section and dump diffuser. The resulting boundary-layer parameter variations through the facility are shown in Figure 7b.¹



a) CFD computational domain



b) Normalized B.L. parameters

Figure 7. C-D nozzle B.L. correction ($R_{th}=5.235$ cm).

In this figure, the line labelled “Trans” is the location where the contour transitions from the 5th order polynomial function to the parabolic function. Between this location and the nozzle exit, the displacement thickness distribution was fit with a 6th order polynomial and the nozzle contour was adjusted for displacement thickness growth. The final step was to reevaluate the 5th order polynomial coefficients to account for the adjusted downstream contour.

Test Section

The test section is basically a constant area cylinder. Two test sections have been fabricated. The first is instrumented with wall static taps and two opposing windows as shown in Figure 8. The primary purpose of the windows is to allow access for probe setup and alignment of the shock generator centerbody. These windows will also be used to evaluate a dynamic skin friction film measurement technique.

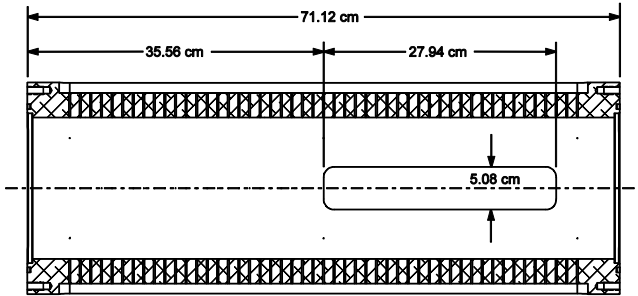


Figure 8. Test section schematic.

The second blank test section is a plain cylinder with provisions to mount the end flanges. This section will be modified at a later date to include optical access for a Particle Image Velocimetry (PIV) system that is currently being designed. A photo of the C-D nozzle and test section are shown in Figure 9. Currently the windows in the test section are aluminum blanks which will be modified to accept additional instrumentation once the extent of the interaction region has been defined. The interior surface of the window is contoured to conform with the circular test section.



Figure 9. C-D nozzle and test section.

Shock Generator

The shock generator (SG) is a cone-cylinder located on the centerline of the wind tunnel as shown in Figure 10. The investigation will initially focus on two SG configurations. Both have a cylinder diameter of 3.135 cm, however, the cone angles differ with one having a half-angle of 10.0° and the other having a half-angle of 13.5° . The former is expected to generate a relatively weak interaction, while the latter will generate a stronger interaction with the possibility of creating boundary-layer separation. The axial placement of the cone tip was chosen so that the conical shock generated by the cone impinges at approximately the center of the window. The window is placed in the downstream half of the test section to minimize the length of the cantilevered SG and also to allow for maximum boundary-layer development.

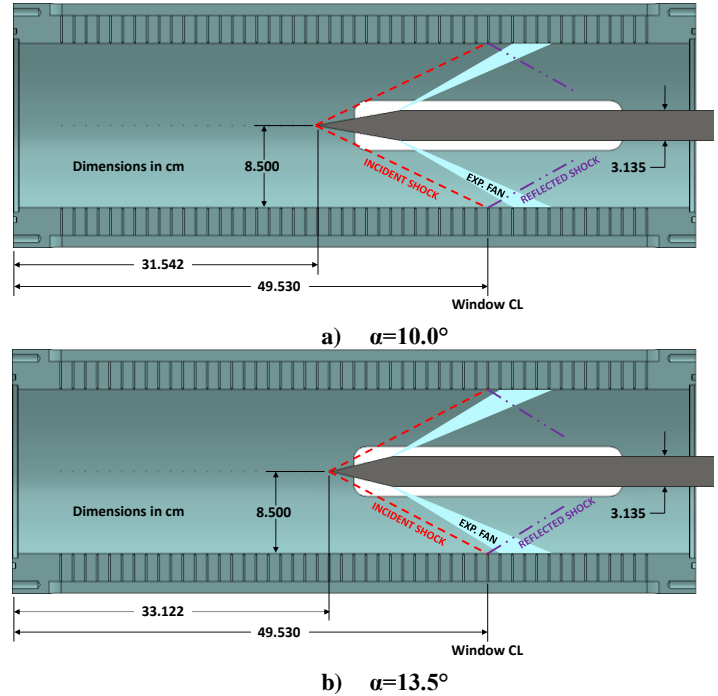


Figure 10. Shock generator schematic.

The centerbody diameter was chosen to minimize blockage of the cantilevered probe configuration. The concern was that in the vicinity of the interaction, the presence of the probe support might cause a local unstart of the wind tunnel. The relatively small centerbody diameter, however, causes close-coupling of the shock-wave and expansion which results in a rapid pressure rise and fall. Once these two baseline interactions are documented, a larger centerbody will be considered as a future test case.

The SG is cantilevered from the end of the test section as shown in Figure 11. For the initial measurements, the cone configuration is

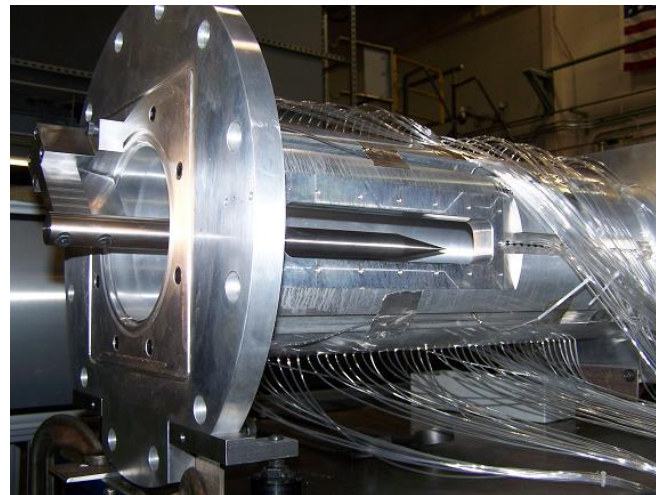


Figure 11. Shock generator assembly.

changed by replacing the entire cone-cylinder. A cylinder with removable tips is currently being designed to allow changing the cone configuration without requiring realignment of the cylinder.

INSTRUMENTATION

For the initial characterization of the interaction regions, conventional pressure instrumentation is used. This consists primarily of wall static pressure taps and Pitot probes for flowfield measurements. Figure 12 shows the general layout of this instrumentation. The throat of the ASME bellmouth has 8 equally spaced static pressure taps. Similarly, the C-D nozzle also has 8 equally spaced static pressure taps located near the exit plane. These taps are located 2.54 cm downstream from the end of the nozzle contour and 3.81 cm upstream of the start of the test section ($x=0$ plane).

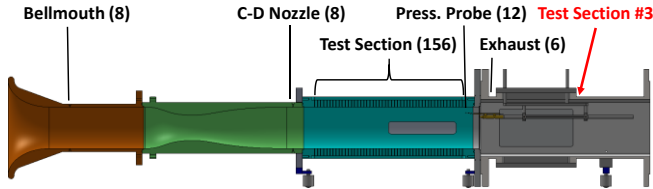


Figure 12. Pressure instrumentation.

The test section has 156 static pressure taps laid out as shown in Figure 13. The first tap for all the stations begins 5.08 cm downstream from the test section inlet plane. Along the top (AA) and bottom (BB), there are 49 equally spaced taps. Along CP and CS there are 23 equally spaced taps. The axial spacing for the taps along AA, BB, CP, and CS are 1.28 cm. There are three equally spaced taps along DP, DS, EP, and ES. The axial spacing at these stations is 35.56 cm.

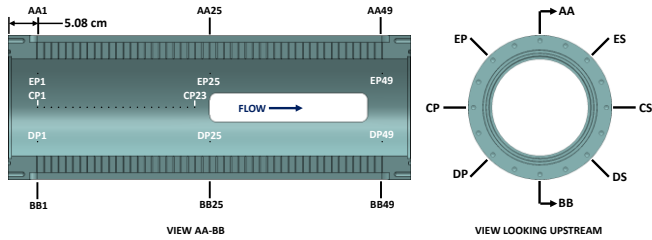


Figure 13. Test section static pressure taps.

With reference to Figure 12, the flow from the circular test section dumps into what is referred to as Test Section #3 which is a 25.4 x 25.4 cm square section. Up to six base pressures can be measured where the flow from the circular test section exits as a free-jet into the square section. Test Section #3 also has a probe traversing capability. Plates on the top and bottom of this section translate in the traverse horizontal direction. An actuator that can be mounted on either the top or bottom plate allows a probe to be translated in the vertical direction. Thus, the combination of these allows a probe to be located anywhere within the test section cross-plane. Both the horizontal and vertical directions are driven by remotely actuated stepper motors. The position of each axis is measured with digital encoders. Currently, positioning the probe in the axial direction is a manual operation.

In addition to surveying in the axisymmetric test section, the facility can also be configured to survey the exit plane of the C-D nozzle. An interior photo of Test Section #3 showing a probe setup for a boundary-layer survey at the C-D nozzle exit is shown in Figure 14. The nose of the probe sting is electrically isolated from the support rod using a nylon threaded rod and washer. This allows probe wall touch to be established by electrical continuity.



Figure 14. C-D nozzle exit plane survey.

In addition to the aforementioned instrumentation, total temperature and total pressure in the plenum chamber are also recorded. Inasmuch as the total temperature is at ambient conditions and can drift over time, the facility controls are setup to automatically adjust the plenum total pressure to maintain a constant Reynolds number.

UNCERTAINTY CONSIDERATIONS

A detailed uncertainty analysis is still in progress but the measurand uncertainties have been estimated and are summarized in Table 1. These uncertainties include the sensor uncertainty as well as the uncertainty associated with the signal processing in the data acquisition system [13]. The variable N represents the number of redundant transducers associated with a measurand. These uncertainties will be combined with estimates of the probe (static tap and Pitot probe) measurement uncertainties which will then be propagated through the calculation procedures.

Table 1. Measurand uncertainty.

i	Description	X_i	δX_i	N	δX_i	Units
1	Plenum total temp.	$T_{t,0}$	1.39	2	0.982	°K
2	Plenum total pressure	$p_{t,0}$	0.0689	1	0.0689	kPa
3	Bellmouth throat static pressure	p_{bm}	0.0255	8	0.0090	kPa
4	Bellmouth throat diameter	D_{bm}	0.0013	1	0.0013	cm
5	Bellmouth discharge coefficient	$C_{D,bm}$	0.0025	1	0.0025	-
6	C-D nozzle exit plane static pressure	p_{noz}	0.0621	8	0.0219	kPa
7	Probe position, x	x_{prb}	0.0064	1	0.0064	cm
8	Probe position, y	y_{prb}	0.0064	1	0.0064	cm
9	Probe position, z	z_{prb}	0.0064	1	0.0064	cm
10	Probe pitot pressure	p_{prb}	0.0621	1	0.0621	kPa

RESULTS AND DISCUSSION

ASME Bellmouth and C-D Nozzle Condition

The facility was initially setup to survey the C-D nozzle exit plane as shown in Figure 14. Prior to performing the surveys, the nozzle Mach number was measured. The Mach number was calculated from the isentropic relation:

$$\text{Eq. 9} \quad M_{noz} = \sqrt{\left(\frac{2}{\gamma-1}\right) \cdot \left(\left(\frac{p_{t,0}}{p_{noz}}\right)^{\frac{\gamma-1}{\gamma}} - 1\right)}$$

where $p_{t,0}$ is the plenum total pressure and p_{noz} is the average of the eight static pressures located at near the nozzle exit. The C-D nozzle exit plane Mach number as a function Reynolds number is shown in Figure 15. The uncertainty in the Mach number measurement based on values in Table 1, which excludes the pressure tap uncertainty, is estimated to be less than 0.05% over the Reynolds number range plotted. The design Mach number of 2.5 is achieved at a Reynolds number of approximately $4.0E+06$. This Reynolds number was subsequently selected as the operating point for the characterization of the facility.

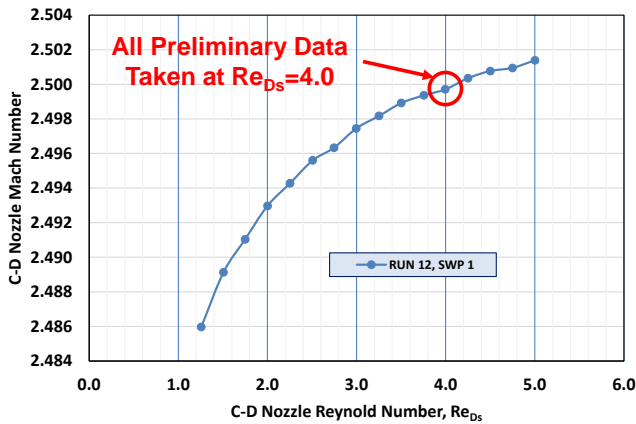


Figure 15. C-D nozzle bulk Mach number.

The mass-flow through the facility was measured with the ASME bellmouth by the method described in Ref. [10]. The mass-flow as a function C-D nozzle Reynolds number is shown in Figure 16. The uncertainty in the mass-flow measurement based on values in Table 1, which excludes the pressure tap uncertainty, is estimated to be less than 0.4% over the Reynolds number range plotted. The mass flow at $Re_{D,noz}=4.0E+06$ is approximately 4.7 kg/s.

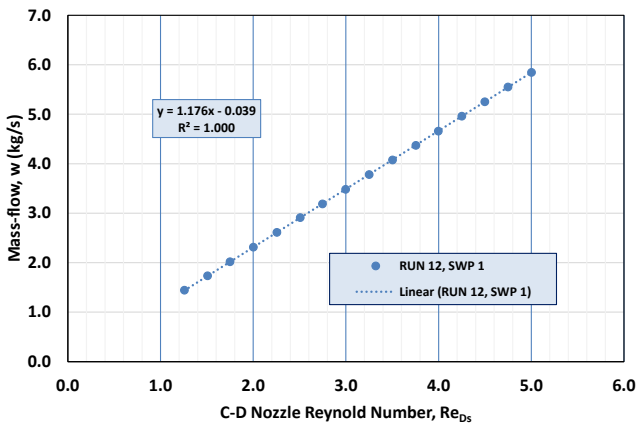


Figure 16. 17 cm Axi-SWT mass flow.

With reference to Figure 13, Pitot pressure surveys were taken along vertical (AA, BB) and horizontal (CP, CS) planes. These surveys,

plotted in terms of Mach number, are shown in Figure 17. From this plot, the core profile is seen to be quite uniform with good agreement with the bulk Mach number from Figure 15. The largest deviation in Mach number occurs near the centerline which is somewhat typical of C-D nozzles.

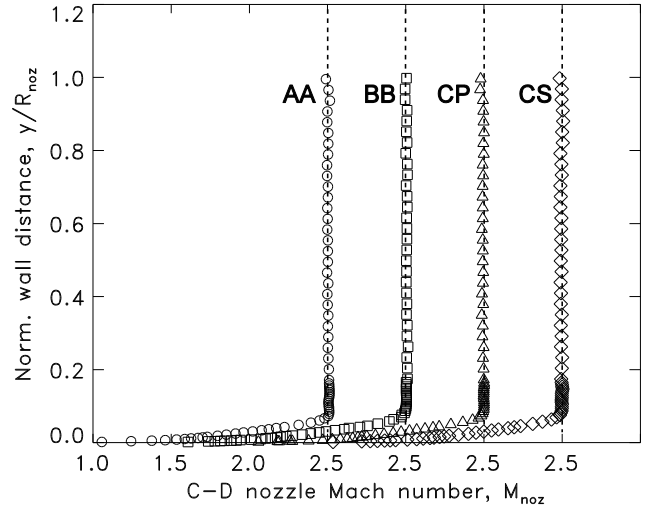


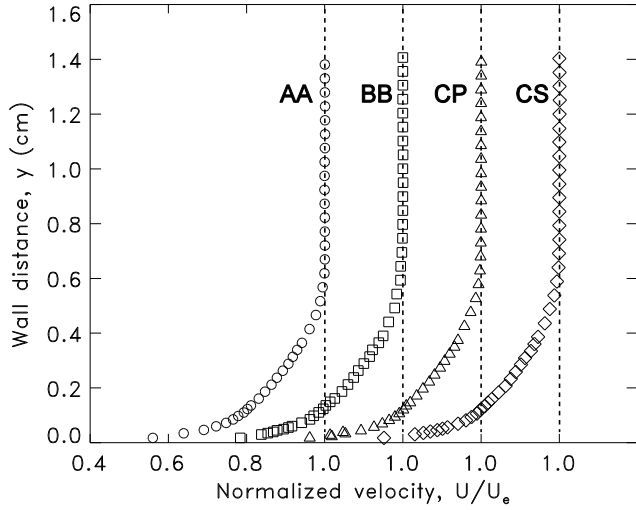
Figure 17. Mach number at C-D nozzle exit, $Re_{Ds,noz}=4.0$.

The boundary-layer region of the profiles shown in Figure 17 was analyzed to calculate relevant boundary-layer parameters. The boundary-layer profiles plotted in terms of velocity normalized by the boundary-layer edge velocity and in terms of van Driest [14] scaled variables are shown in Figure 19a and Figure 19b, respectively. With reference to Figure 19b, the profiles generally follow the law-of-the-wall, but perhaps with a slightly elevated slope which is likely a result of distortion by the strong favorably pressure gradient in the nozzle. The average boundary-layer parameters from the four profiles are summarized in Table 2 (EXP, $x=-3.81$ cm). Also shown in this table for comparison are the results of the WIND CFD analysis (WIND, $x=-3.81$) used to correct the nozzle contour. Note that this is an approximate comparison since the WIND results were for the inviscid nozzle contour which results in a slightly lower Mach number.

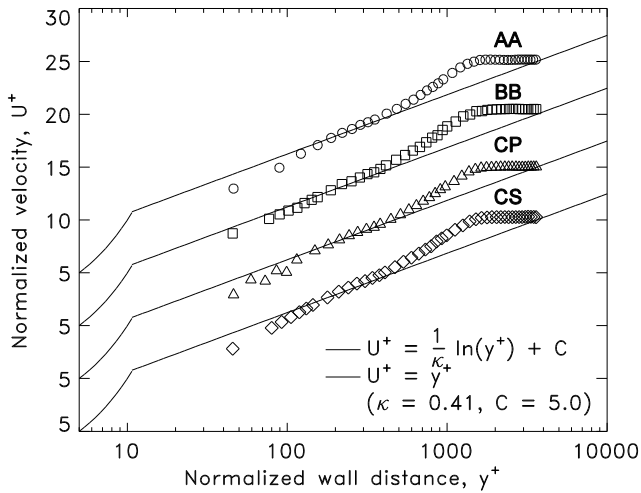
Table 2. Boundary-layer parameters.

	x (cm)	M_e	δ (cm)	δ^* (cm)	θ (cm)	H_i	C_f
WIND	-3.81	2.46	0.693	0.162	0.041	-	-
EXP	-3.81	2.50	0.608	0.161	0.041	1.39	0.00186
EXP	43.2	2.44	1.312	0.334	0.090	1.33	0.00157
EXP	66.0	2.44	1.465	0.389	0.106	1.31	0.00152

The measured boundary-layer thickness at the nozzle exit is approximately 0.61 cm, which is somewhat thinner than the results of the WIND analysis (0.69 cm). The integral properties, however, are in quite good agreement. The incompressible shape factor at the nozzle exit, which is typically about 1.3 for a fully turbulent, zero pressure gradient boundary layer, is slightly elevated and likely a result of the transition from strong favorable pressure gradient to mild adverse pressure gradient at the nozzle exit.



a) Normalized velocity profile



b) Law-of-the-wall

Figure 19. Boundary-layer profiles at C-D nozzle exit.

Shock-Free Flow through Test Section

After completion of the preliminary measurements of the nozzle, the facility was reconfigured with the test section as shown in Figure 4b. Without a shock generator, the flow through the test section is supersonic developing pipe flow with friction, or Fanno line flow.

Wall static pressure distributions at a Reynolds number of $Re_{Ds,noz} = 4.0$ are shown in Figure 18.² As expected, the pressure rises slightly through the test section. There is observed to be some slight scatter in the data and also slight differences between the upper (AA) and lower (BB) distributions in the second half of the test section. This will be investigated further by checking alignment with the nozzle and also by rotating the test section 180° and repeating the measurements. In fact, one aspect of this investigation will be to document and quantify the sensitivity of the results to tunnel assembly procedure and configuration.

With reference to Figure 13, Pitot pressure surveys were taken along vertical (AA, BB) and horizontal (CP, CS) planes at the last static

pressure tap location ($x=66.0$ cm) at a scaled Reynolds number of $Re_{Ds,noz}=4.0$. These surveys, plotted in terms of Mach number, are shown in Figure 20. At this station the Mach number in the core has dropped to about 2.4. The profiles at CP and CS show a slightly higher than core point at the edge of the boundary layer which is absent from the profiles at AA and BB. This has been traced to a small forward facing step at the downstream end of the window. The windows are currently being modified to eliminate this step.

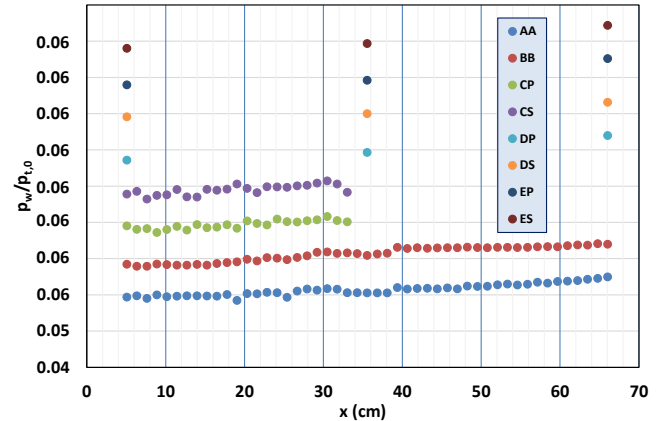


Figure 18. Wall pressure distribution through test section.

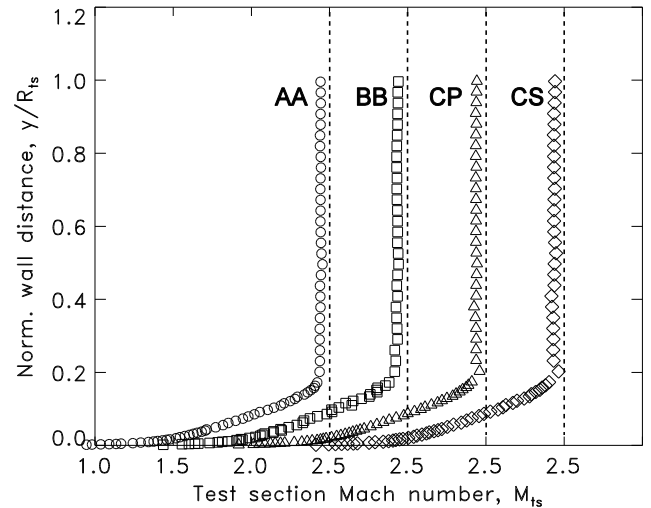
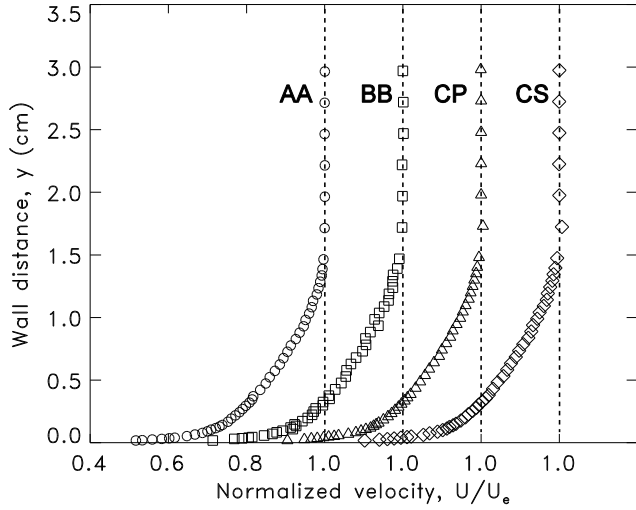


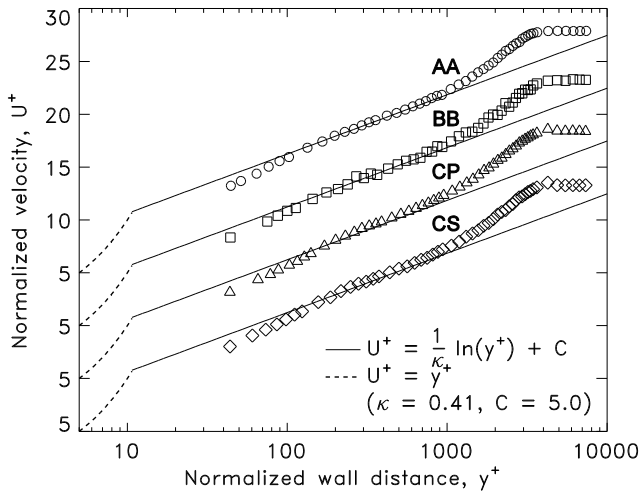
Figure 20. Mach number at test section exit, $Re_{Ds,noz}=4.0$.

The boundary-layer profiles at the test section exit plotted in terms of velocity normalized by the boundary-layer edge velocity and in terms of van Driest [14] scaled variables are shown in Figure 21a and Figure 21b, respectively. The average boundary-layer parameters at the test section are summarized in Table 2. The edge Mach number is reduced to $M=2.38$ and the boundary-layer thickness has approximately doubled through the test section to 1.37 cm. The profiles used to accumulate these data were the same as the profiles at the nozzle exit and it can be seen that there is a lack of resolution at the boundary-layer edge. These profiles will be repeated as part of the quest for high fidelity measurements. With reference to Figure 21b, the profiles, which have been developing in a mild adverse pressure gradient, follow the theoretical law-of-the-wall better than the nozzle exit profiles.

² For clarity, the distributions are shifted by $P_w/P_{t,0}=0.01$.



a) Normalized velocity profile

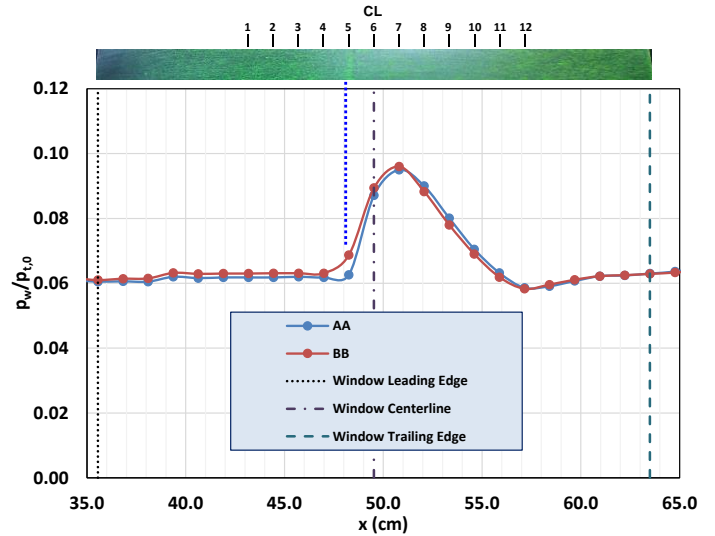


b) Law-of-the-wall

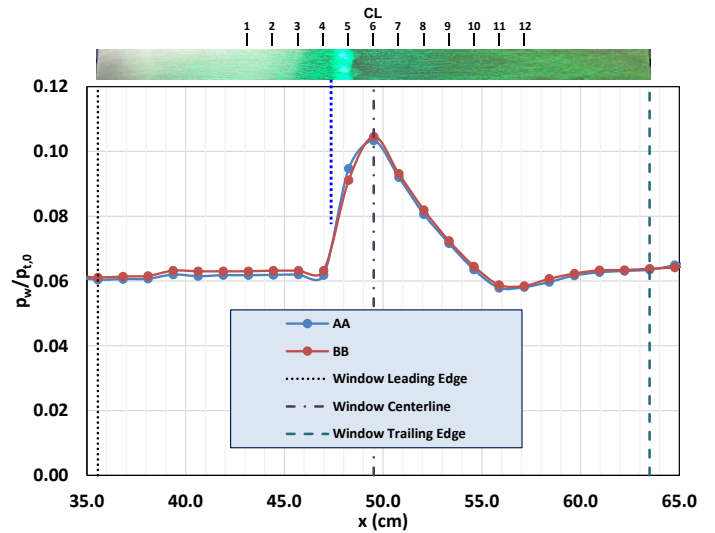
Figure 21. Boundary-layer profiles at test section exit.

Flow through Test Section with Shock Interaction

The final set of preliminary measurements was performed with the two shock generator configurations shown in Figure 10. The wall static pressure distributions on the upper (AA) and lower (BB) positions are shown for the 10.0° and 13.5° shock generators in Figure 22a and Figure 22b, respectively. To estimate the shock impingement location, surface flow visualization was performed using an oil and fluorescent dye mixture. These results are shown at the top of the figures. For both cases, symmetry between the upper and lower pressure tap positions is observed to be quite good. As anticipated, the interaction region for both cases is located in the vicinity of the window centerline. The magnitude of the peak pressure and the axial extent of the interaction region is, as expected, greater for the stronger interaction case. For the 10.0° case, the oil flow shows a light line indicating the upstream influence of the shock impingement, but no flow separation appears to be present. This line also corresponds with the initial rise in wall pressure. For the 13.5° case, the oil flow shows a small pooling of oil indicating flow separation. The upstream edge of the pooling also corresponds with the initial rise in wall pressure.



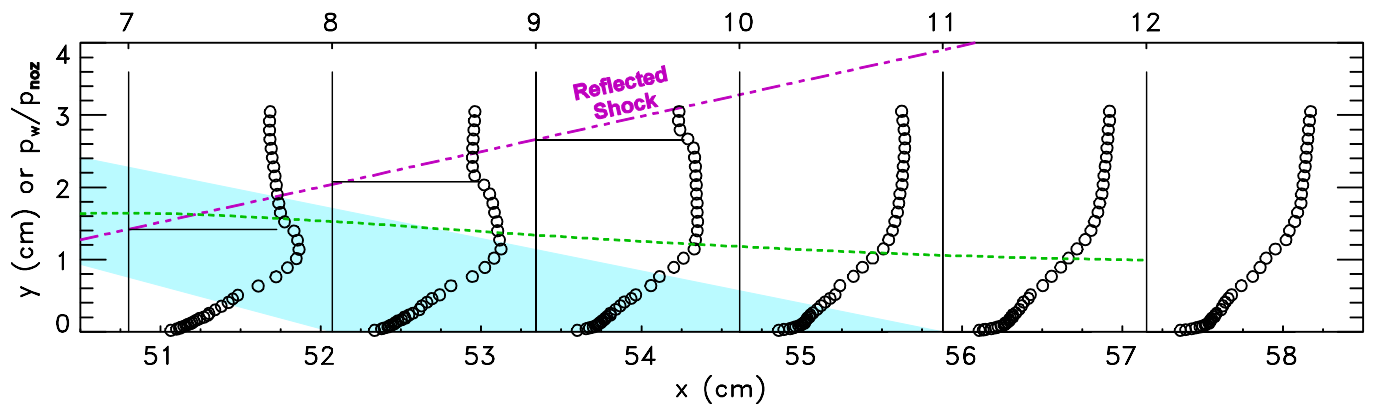
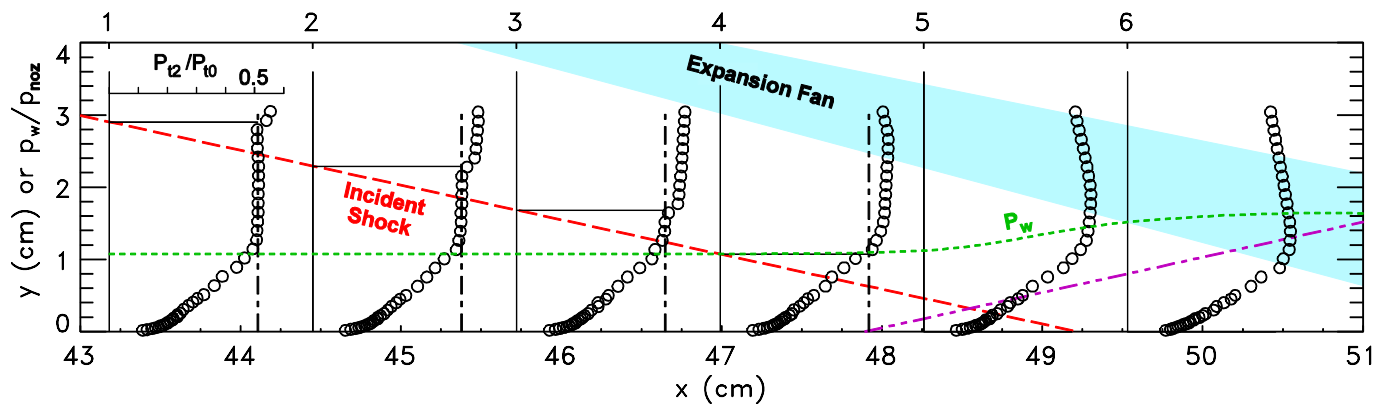
a) $\alpha=10.0^\circ$



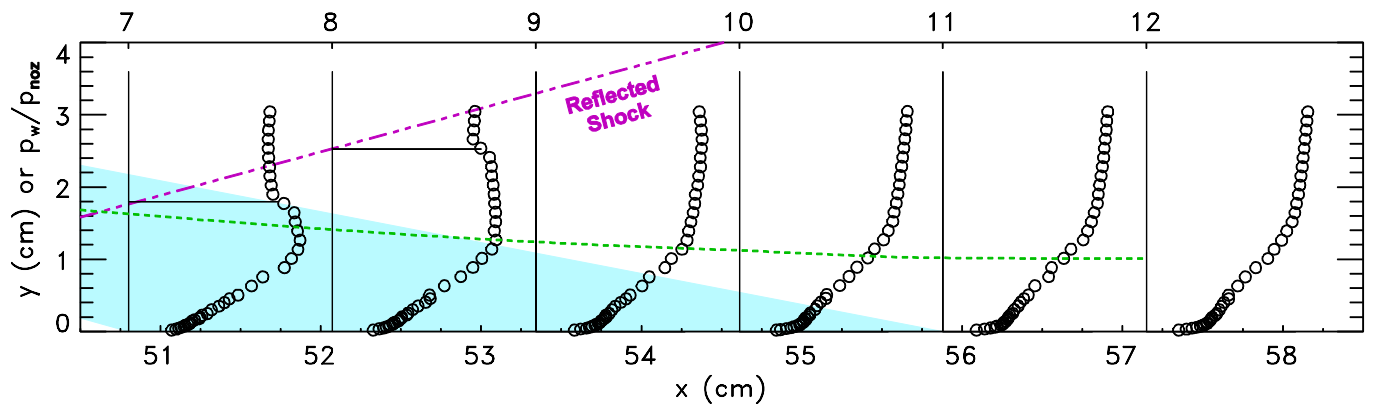
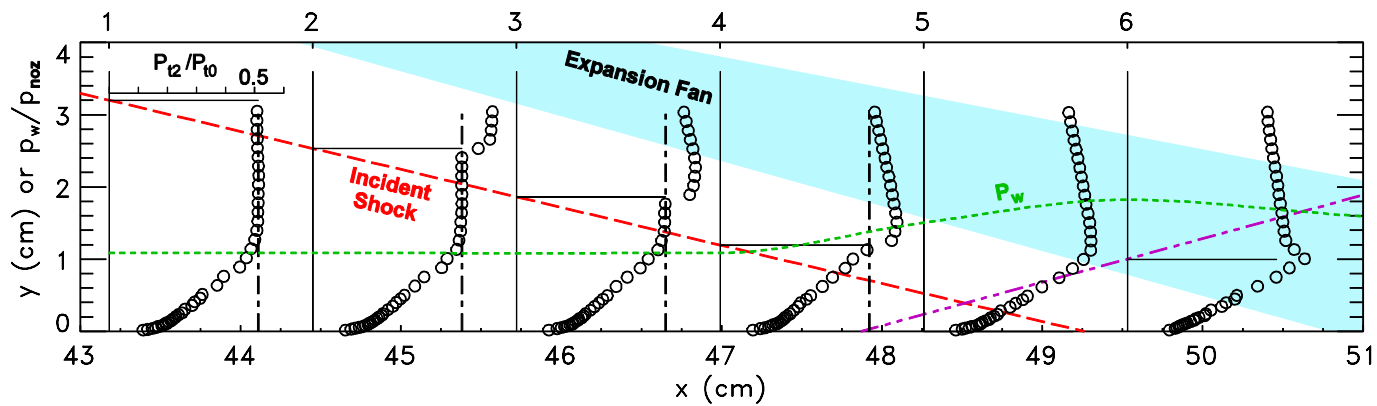
b) $\alpha=13.5^\circ$

Figure 22. Wall pressure through interaction region.

Pitot pressure profiles were taken at twelve axial stations through the interaction region at position BB for the $\alpha=10.0^\circ$ and 13.5° cases. The location of the profiles are indicated in Figure 22 and the profiles at all 12 stations are shown in Figure 23. The first profile is located at $x=43.2$ cm and the remaining profiles are equally spaced at 1.28 cm increments. The profiles plotted are the Pitot pressure normalized by the plenum total pressure. The wall static pressure normalized by the nozzle exit static pressure (P_w/P_{noz}) is also plotted as a dotted line. At the first station it is reasonable to assume that the wall static pressure is constant across the boundary-layer. Boundary-layer parameters were calculated for this station and are summarized in Table 2. One of the conclusions from Ref. [8] is that when the ratio of upstream boundary-layer thickness to duct radius is greater than 0.1, a planar two-dimensional analysis cannot be used to predict flow separation because changes in the boundary-layer properties are larger for conical incident shock waves in an axisymmetric duct. For the present case, the ratio of boundary-layer thickness to duct radius is 0.154 indicating that the axisymmetric analysis must be used.



a) $\alpha=10.0^\circ$



b) $\alpha=13.5^\circ$

Figure 23. Pitot profiles development through interaction region, $Re_{DS,noz}=4.0$.

The incident shock plotted in the figures is based on inviscid theory using the cone angle and Mach number at the cone tip. This cone tip Mach number was interpolated from measurements made at the nozzle and test section exits. For the first four profiles, horizontal lines are drawn from where the incident shock crosses the data station to the Pitot profile. For both cases, these lines are in excellent agreement with the shock position indicated by the Pitot probe. Also indicated by vertical lines on the first four profiles is the normal shock total pressure ratio associated with Mach number at the cone tip. This agrees well with the measured normalized Pitot pressure below the incident shock.

The reflected shock shown in the plots is based on the location inferred from the Pitot pressure profiles. As expected, the presence of the boundary layer moves the virtual origin of the reflected shock upstream of the incident shock impingement location.

CONCLUDING REMARKS

A new facility for investigating a Mach 2.5, 2-D shock-wave boundary-layer interaction has been presented along with preliminary measurements characterizing the flowfield. The data generated, once vetted by uncertainty estimates and redundant measurements, is intended to be used for CFD validation efforts. The preliminary results indicate that the facility is suitable for this purpose. From these preliminary data, refined flowfield measurement stations and surface dynamic pressure locations will be identified. Once the mean flow field has been characterized by conventional pressure measurements, constant-voltage hot-wire anemometry and PIV will be used to characterize the turbulence field throughout the interaction region

ACKNOWLEDGMENTS

Funding from the Transformational Tools & Technologies Project of the NASA Transformative Aeronautics Concept Program is gratefully acknowledged.

REFERENCES

- [1] Settles, G. S., and Dodson, L. J., 1994, "Supersonic and Hypersonic Shock/Boundary-Layer Interaction Database," *AIAA Journal*, Vol. 32, No. 7, pp. 1377-1383.
- [2] Settles, G. S., and Dodson, L. J., 1991, "Hypersonic Shock/Boundary-Layer Interaction Database," NASA CR 177577.
- [3] Aeschliman, D. P., and Oberkampf, W. L., 1998, "Experimental Methodology for Computational Fluid Dynamics Code Validation," *AIAA Journal*, Vol. 36, No. 5, pp. 733-741.
- [4] Benek, A. J., Suchyta, C. R., and Babinsky, H., 2013, "The Effect of Wind Tunnel Size on Incident Shock Boundary Layer Interaction Experiments," AIAA Paper 2013-0862, 51st AIAA Aerospace Sciences Meeting, Grapevine, TX.
- [5] Bruce, P. J. K., Burton, D. M. F., Titchener, N. A., and Babinsky, H., 2011, "Corner Effect and Separation in Transonic Channel Flows," *J. Fluid Mechanics*, Vol. 679, pp. 247-262.
- [6] Rose, W. C., 1973, "The Behavior of a Compressible Turbulent Boundary Layer in a Shock-Wave-Induced Adverse Pressure Gradient," NASA TN D-7092.
- [7] Seebaugh, W. R., Paynter, G. C., and Childs, M. E., 1968, "Shock-Wave Reflection from a Turbulent Boundary Layer with Mass Bleed," *J. Aircraft*, Vol. 5, No. 5, pp. 461-467.
- [8] Seebaugh, W. R., and Childs, M. E., 1970, "Conical Shock-Wave Turbulent Boundary-Layer Interaction Including Suction Effects," *J. Aircraft*, Vol. 7, No. 4, pp. 334-340.
- [9] Bean, H. S. (ed), 1971, *Fluid Meters: Their Theory and Application*, 6th Ed., American Society of Mechanical Engineers, New York.

[10] Davis, D. O., Friedlander, D. J., Saunders, J. D., Frate, F. C., and Foster, L., 2012, "Calibration of the NASA GRC 16" Mass Flow Plug," FEDSM2012-72266, 2012 ASME Fluids Engineering Division Summer Meeting, Puerto Rico, USA.

[11] Towne, C., "Wind-US User's Guide, Version 2.0," Glenn Research Center, NASA/TM-2009-215804, Oct. 2009.

[12] Menter, F.R., "Two-Equation Eddy Viscosity Turbulence Models for Engineering Applications," *AIAA Journal*, Vol. 32, No. 8, 1994, pp. 1598-1605.

[13] Blumenthal, P.Z., 1995, "A PC Program for Estimating Measurement Uncertainty for Aeronautics Test Instrumentation," AIAA Paper 1995-3072, 31st AIAA Joint Propulsion Conference and Exhibit, San Diego, CA.

[14] van Driest, E. R., 1951, "Turbulent Boundary Layer in Compressible Fluids," *J. Aeronautical Sciences*, Vol. 18, pp. 145-160.